Functional Importance of Tyrosine 294 and the Catalytic Selectivity for the Bis-Fe(IV) State of MauG Revealed by Replacement of This Axial Heme Ligand with Histidine

ARTICLE *in* BIOCHEMISTRY · OCTOBER 2010

Impact Factor: 3.02 · DOI: 10.1021/bi101254p · Source: PubMed

6 AUTHORS, INCLUDING:

Nafez Abu Tarboush
University of Jordan
7 PUBLICATIONS **94** CITATIONS
SEE PROFILE

Manliang Feng
Tougaloo College
20 PUBLICATIONS **430** CITATIONS
SEE PROFILE

Victor L Davidson
University of Central Florida
219 PUBLICATIONS **5,295** CITATIONS
SEE PROFILE

Published in final edited form as:
Biochemistry. 2010 November 16; 49(45): 9783–9791. doi:10.1021/bi101254p.

Functional importance of Tyrosine294 and the catalytic selectivity for the *bis*-Fe(IV) state of MauG revealed by replacement of this axial heme ligand with Histidine[†,‡]

Nafez Abu Tarboush[1], **Lyndal M. R. Jensen**[2], **Manliang Feng**[1], **Hiroyasu Tachikawa**[3], **Carrie M. Wilmot**[2], and **Victor L. Davidson**[1]

[1]Department of Biochemistry, University of Mississippi Medical Center, Jackson, MS 39216

[2]Department of Biochemistry, Molecular Biology and Biophysics, University of Minnesota, 321 Church St. SE, Minneapolis, MN 55455

[3]Department of Chemistry, Jackson State University, Jackson, MS 39217

Abstract

The diheme enzyme MauG catalyzes the posttranslational modification of a precursor protein of methylamine dehydrogenase (preMADH) to complete the biosynthesis of its protein-derived tryptophan tryptophylquinone (TTQ) cofactor. It catalyzes three sequential two-electron oxidation reactions which proceed through a high valent *bis*-Fe(IV) redox state. Tyr294, the unusual distal axial ligand of one *c*-type heme, was mutated to His and the crystal structure of Y294H MauG in complex with preMADH reveals that this heme now has His-His axial ligation. Y294H MauG is able to interact with preMADH and participate in inter-protein electron transfer, but it is unable to catalyze the TTQ biosynthesis reactions that require the *bis*-Fe(IV) state. This mutation not only affects the redox properties of the six-coordinate heme but also the redox and CO-binding properties of the five-coordinate heme, despite the 21 Å separation of the heme iron centers. This highlights the communication between the hemes which in wild-type MauG behave as a single diheme unit. Spectroscopic data suggest that Y294H MauG can stabilize a high valent redox state equivalent to Fe(V), but it appears to be an Fe(IV)=O/π radical at the five-coordinate heme rather than the *bis*-Fe(IV) state. This compound I-like intermediate does not catalyze TTQ biosynthesis, demonstrating that the *bis*-Fe(IV) state, which is stabilized by Tyr294, is specifically required for

[†]This work was supported by NIH grants GM-41574 (VLD), GM-66569 (CMW), RCMI G12RR13459 (HT) and Minnesota Partnership for Biotechnology and Medical Genomics Grant SPAP-05-0013-P-FY06 (CMW)

[‡]Co-ordinates and structure factors have been deposited in the Protein Data Bank as entry 3ORV

Address correspondence to: Victor L. Davidson, Department of Biochemistry, University of Mississippi Medical Center, 2500 N. State St., Jackson, MS 39216-4505. Tel: 601-984-1516. Fax: 601-984-1501. vdavidson@umc.edu.

[1]Abbreviations:

MADH	methylamine dehydrogenase
TTQ	tryptophan tryptophylquinone
preMADH	the biosynthetic precursor protein of MADH with incompletely synthesized TTQ
ET	electron transfer
***bis*-Fe(IV) MauG**	redox state of MauG with one heme as Fe(IV)=O and the other as Fe(IV)
E_m	oxidation-reduction midpoint potential
WT	wild type
PDB	Protein Data Bank

this reaction. The TTQ biosynthetic reactions catalyzed by wild-type MauG do not occur via direct contact with the Fe(IV)=O heme, but via long range electron transfer through the six-coordinate heme. Thus, a critical feature of the *bis*-Fe(IV) species may be that it shortens the electron transfer distance from preMADH to a high valent heme iron.

Tyrosine participates in a variety of important functions in a wide range of different proteins and enzymes. It is the site of reversible phosphorylation by tyrosine kinases which regulate the activity of several enzymes that are part of signal transduction processes (1). Tyrosine plays a catalytic role in the active sites of certain enzymes, and in some enzymes is posttranslationally modified to generate protein-derived cofactors (2). Tyrosine is the most frequently reported site for the occurrence of free radicals in proteins (3). This ability of tyrosine to stabilize free radicals in proteins is widespread in nature. For example, it is critical to the functions of photosystem II in photosynthesis (4), cytochrome *c* oxidase in respiration (5), and ribonucleotide reductase in metabolism (6). Tyrosine residues have also been implicated in the propagation of Alzheimer's and Parkinson disease (7).

At heme sites in proteins the ability of tyrosine to form stable radicals has important biological consequences that may be advantageous or deleterious (8). Introduction of tyrosine at the heme site of proteins by site-directed mutagenesis studies has been shown to alter the properties and reactivity of the heme. In cytochrome b_5, the V45Y mutation in the heme pocket resulted in a 25 mV decrease of its redox potential (9). For *iso*-1-cytochrome *c*, the Y67F mutation enhanced resistance to H_2O_2-induced heme degradation (10). For cytochrome *c* peroxidase, mutation of the catalytic His52 to tyrosine permits the formation of a crosslink between Tyr52 and Trp51, and this was accompanied by a decrease in the rate of formation of Compound 1 of five orders of magnitude (11). In human cytochrome b_{558}, a naturally occurring mutation of the putative axial heme ligand His101 to tyrosine caused loss of NADPH oxidase activity of phagocytes, which leads to recurrent bacterial infections in humans and a condition known as X-linked chronic granulomatous disease (12). Another His to Tyr mutation in this oxidase, also believed to alter a heme ligand, has been implicated in the progression of atherosclerotic coronary artery disease (13).

A significant but less common role of tyrosine is the provision of an axial ligand for the heme iron in certain heme-containing enzymes such as the *b*-type heme in catalase (14), where it can stabilize high valent iron species. Tyrosine has recently been identified as an axial ligand of the six-coordinate heme (15) of an unusual diheme enzyme, MauG from *Paracoccus denitrificans* (16), which catalyzes the biosynthesis of the protein-derived tryptophan tryptophylquinone (TTQ) cofactor (17) of methylamine dehydrogenase (MADH) (18). The substrate for MauG is an MADH precursor protein (preMADH) in which residue βTrp57 has been monohydroxylated (19). MauG catalyzes the six-electron oxidation of preMADH which results in a second hydroxylation of βTrp57, crosslinking of βTrp57 to βTrp108, and oxidation of the quinol species to the quinone (20,21) (Scheme 1). The axial ligands for the six-coordinate heme are His205 and Tyr294 and the sole axial ligand for the five-coordinate heme is His35 (15). The diheme system of MauG exhibits redox cooperativity and the two hemes behave as a single diheme unit rather than independent hemes with no formation of a formal Fe(II)-Fe(III) mixed valence state (22). A novel feature of MauG is that on reaction with H_2O_2 it generates a relatively stable *bis*-Fe(IV) state with the five-coordinate heme as Fe(IV)=O and the other heme as Fe(IV) with the two axial ligands from the protein retained (23).

Natural Tyr-His heme *c* ligation has not previously been described, and MauG is the first known example of a *c*-type heme with axial ligation by tyrosine. Tyr294 is a conserved residue in the known MauG sequences (15). This unprecedented axial ligation of the six-coordinate heme of MauG suggests that it endows this *c*-type heme with specific properties

necessary for catalysis of TTQ formation. In this study, replacement of Tyr294 with histidine results in His-His axial ligation that is shown to significantly alter the spectroscopic, redox and catalytic properties of MauG. This mutation not only affects the properties of the six-coordinate heme, but also the redox, CO-binding properties and high valence state of the five-coordinate heme, despite the fact that the two heme irons are separated by 21 Å. These results establish that Tyr294 is critical for stabilization of the *bis*-Fe(IV) redox state and that this unusual high valence state is specifically required for TTQ biosynthesis.

Experimental Procedures

Protein Expression and Purification

Methods for the expression and purification of MADH (24), preMADH (19), and MauG (16) were as described previously. Protein concentrations were calculated using the following extinction coefficients: diferric MauG (ε_{406} = 309.0 $mM^{-1}cm^{-1}$), quinone MADH (ε_{440} = 26.2 $mM^{-1}cm^{-1}$), quinol MADH (ε_{330} = 56.4 $mM^{-1}cm^{-1}$) and preMADH (ε_{280} = 157 $mM^{-1}cm^{-1}$). Site-directed mutagenesis to create Y294H MauG was performed on double-stranded pMEG391 (16), which contains *mauG*, using forward and reverse mutagenic primers with the Quikchange site-directed mutagenesis kit (Strategene). The entire *mauG*-containing fragment was sequenced to ensure that no second site mutations were present. Y294H MauG was expressed in *P. denitrificans* cells and isolated from the periplasmic fraction as described for recombinant wild-type (WT) MauG (16). The yield of the protein was 1.1 mg/L of culture for Y294H MauG. The extinction coefficient of Y294H MauG was determined by the pyridine hemochrome method (25).

Redox Titrations

Reference absorption spectra for diferrous and diferric WT MauG and Y294H MauG were determined by reduction with sodium dithionite and oxidation with potassium ferricyanide under anaerobic conditions. The oxidation-reduction midpoint potential (E_m) values were determined by anaerobic spectrochemical titration as described previously for WT MauG (22) using flavin mononucleotide as a mediator. The titrations were fully reversible. The ratio of oxidized/reduced protein after incremental additions of dithionite or ferricyanide was determined by comparison with the spectra of the completely oxidized and reduced forms of MauG, after the absorbance of the mediator was subtracted from the recorded spectrum. E_m values were obtained by fitting the experimental data to eq 1, which describes the redox behavior of a system with two redox active centers where *a* is the fraction of the total absorbance change attributable to one heme and (1 – a) is the fraction of the total absorbance change attributable to the other heme. E_m values are reported versus the normal hydrogen electrode.

$$\text{Fraction reduced} = a / \left[1 + 10^{((E-Em1)/0.059V)}\right] + (1-a) / \left[1 + 10^{((E-Em2)/0.059V)}\right] \quad (1)$$

CO Binding Studies

Diferrous Y294H MauG was prepared in deoxygenated 0.01 M potassium phosphate (pH 7.5) and quantitatively reduced by anaerobic addition of sodium dithionite. A stock solution of CO-saturated buffer (930 μM at 25 °C) was prepared by bubbling O_2-free N_2 for 4 hr through the 10 mM potassium phosphate, pH 7.5, and then flushing with CO for 45 min as described previously (26). Solutions with various concentrations of CO were prepared by diluting the stock solution with deoxygenated buffer. The reaction was studied using an Online Instrument Systems (OLIS, Bogart, GA) RSM rapid-scanning stopped-flow

spectrophotometer. One syringe contained the diferrous Y294H MauG and the other syringe contained buffer with varying concentrations of CO. The final concentration of protein after mixing was 2 μM. Reactions were monitored between 366 nm and 446 nm. In each reaction, data were best fit to a two-phase exponential transition.

Resonance Raman Spectroscopy

Resonance Raman spectra were recorded using a Spex model 1877 triple spectrograph Raman spectrometer equipped with a CCD detector as reported previously (22). Samples were prepared in 50 mM potassium phosphate, pH 7.5 at 25 °C. Samples were frozen using liquid nitrogen before and immediately after addition of H_2O_2. A 406.7 nm line from an argon-krypton ion laser (Spectra-Physics BeamLok model 2080-KV) was used as the excitation source, and the Raman signal was collected in a 120° geometry. The laser power was adjusted to ~5 mW at the sample. Each spectrum was recorded with a 60 s accumulation time, and 10 repetitively measured spectra. The wavenumbers of the Raman bands in the spectra of the samples were calibrated using the spectrum of cyclohexane as a standard.

Assays for Y294H MauG-dependent TTQ Biosynthesis

Steady state kinetic studies of MauG-dependent TTQ biosynthesis from preMADH (Scheme 1) were performed using a previously described spectrophotometric assay (27). H_2O_2, or dithiothreitol with O_2, were each tested as the source of oxidizing equivalents in the steady state assay. Y294H MauG (0.5 μM) was mixed with preMADH (5 μM) in 0.01 M potassium phosphate buffer, pH 7.5 at 25 °C. Reactions were initiated by addition of 100 μM H_2O_2 or 250 μM dithiothreitol and the rate of appearance of quinone MADH was monitored at 440 nm. The same steady state assay was used to assay Y294H MauG-dependent TTQ biosynthesis from quinol MADH (28).

Assay for Electron Transfer (ET) from Diferrous Y294H MauG to Quinone MADH

The single-turnover kinetics of the reaction of diferrous Y294H MauG with quinone MADH were studied as described previously for WT MauG (28). Reaction mixtures contained a fixed concentration of diferrous Y294H MauG (1.25 μM). This was mixed with varied concentrations of quinone MADH. Reactions were performed under anaerobic conditions to ensure that the MauG remained reduced prior to and during reaction with MADH. The reaction was monitored by the decrease in absorbance at 550 nm which corresponds to the conversion of diferrous Y294H MauG to diferric MauG (16). Data were analyzed using equations 2 and 3 where S is quinone MADH, E is diferrous MauG, E' is diferric MauG, and P is quinol MADH.

$$E+S \leftrightharpoons^{K_d} ES \leftrightharpoons^{K_4}_{K_3} EP \tag{2}$$

$$k_{obs}=k_3\,[S]\,/\,([S]+K_d)+k_4 \tag{3}$$

Crystallization and X-Ray Structure Determination of the Y294H MauG/preMADH Complex

Y294H MauG was co-crystallized with preMADH from a protein solution containing 100 μM Y294H MauG and 50 μM preMADH in 10 mM potassium phosphate, pH 7.5, as the WT MauG/preMADH molecular complex has a 2:1 MauG/preMADH ratio. The Y294H MauG/preMADH complex crystallized through optimization of the conditions already established for WT MauG/preMADH by hanging drop vapor diffusion in VDX plates (Hampton Research) (15). Single crystals suitable for X-ray data collection were obtained

from drops assembled with 1 μL protein solution/2 or 3 μL reservoir solution over a 22-26 % (w/v) PEG 8000, 0.1 M sodium acetate, 0.1 M MES pH 6.4 reservoir. Crystals were cryoprotected as described previously through the inclusion of 10 % PEG 400 (15). X-ray diffraction data were collected at GM/CA-CAT beamline 23-ID-D of the Advanced Photon Source (APS), Argonne National Laboratory, Argonne, IL. A 360° dataset was collected at 100 K from a crystal with dimensions ~ 180 × 50 × 15 μm. The diffraction data were essentially isomorphous with data obtained from WT MauG/preMADH crystals, and are in the space group *P*1with one complex (two Y294H MauG bound to one preMADH) in the asymmetric unit. The data were processed with HKL2000, and extended to 1.92 Å resolution (29).

The structure solution was obtained by difference Fourier. Refinement was carried out using REFMAC (30) in the CCP4 program suite (31) and model-building was carried out in COOT (32). The initial model used the coordinates of WT MauG/preMADH (PDB entry 3L4M) retaining only the protein and solvent components and with residue 294 of MauG truncated to Ala. Restrained refinement with TLS was carried out using no distance restraints between the heme irons and their ligands. The His294 was well-ordered, and added to the model based on the 2Fo-Fc and Fo-Fc electron density maps. Some rebuilding was required during refinement to assign all residues in the C-terminal regions of both Y294H MauG copies where significant structural changes had occurred relative to WT MauG. Refinement was assessed as complete when the Fo-Fc electron density contained only noise.

Results

Effects of the Y294H Mutation on the Visible Absorption Spectra of Diferric and Diferrous MauG

It should be noted that since MauG is a diheme protein, its spectral features represent a combination of contributions from each heme. Anaerobic titration of Y249H MauG with sodium dithionite confirmed that two electron equivalents are required for conversion of the diferric to the diferrous state (data not shown). The spectra of the diferrous and diferric forms reveal that the Y294H mutation caused subtle changes in the absorption maxima of the α, β and Soret peaks of MauG, as well as significant changes in the extinction coefficients for the peaks. The magnitude of the reduced minus oxidized extinction coefficients for the Soret peak was much greater for Y294H MauG than for WT MauG (Figure 1). The extinction coefficients for the α and β peaks of reduced Y294H MauG were also larger than those of WT MauG (Table 1). Another distinction is that the spectrum of diferrous WT MauG displays a shoulder at 427 nm which is absent in the spectrum of diferrous Y294H MauG.

Effect of the Y294H Mutation on the E_m Values of MauG

MauG exhibits two E_m values which correspond to the sequential addition or removal of the first and second electron from the diheme system. The Y294H mutation caused significant changes to both E_m values (Table 2). It is evident from the redox titrations (Figure 2) that the separation of the two E_m values is much greater in Y294H MauG (−17 mV and −377 mV) than in WT MauG (−158 mV and −246 mV). Thus, the mutation is affecting both E_m values for this diheme system.

Effect of the Y294H Mutation on CO Binding to Diferrous MauG

Carbon monoxide (CO) is a useful O_2 analog that may be used to probe the relative binding affinity of ferrous heme towards O_2. The kinetics of CO binding towards WT MauG have been previously reported (26) and EPR studies of the interaction of NO with MauG have

confirmed that this exogenous ligand binds to only one of the hemes (33). The reaction of WT diferrous MauG with CO was biphasic with a rapid major phase that exhibited a linear dependence on [CO] and a slow minor phase of 16 s^{-1} that was independent of [CO] and was attributed to a conformational change that occurred after CO binding (26). The reaction of Y294H MauG was also biphasic. A slow [CO]-independent phase was observed with a rate of 10 s^{-1}. The faster major phase exhibited a linear dependence on [CO] (Figure 3). Analysis of the data for the [CO]-dependent reaction yielded a kinetically determined K_d of 12 μM for CO binding to Y294H MauG. This was 14-fold less than the K_d value for CO binding to WT MauG (Table 2). Thus, while Tyr294 provides a ligand for the six-coordinate heme of MauG, the Y294H mutation significantly affected the binding of CO to the five-coordinate heme.

Effect of the Y294H Mutation on Reaction of MauG with H_2O_2

It was previously shown that reaction of diferric MauG with H_2O_2 resulted in the formation of a relatively stable *bis*-Fe(IV) species which was reactive towards preMADH (23). The formation and decay of this high valent species is accompanied by changes in the visible absorption spectrum of MauG (26). Reaction of Y294H MauG with H_2O_2 also caused changes in the visible absorption spectrum, but with different characteristics to those observed for WT MauG. Upon reaction of WT MauG with H_2O_2 the Soret band displays a red-shift of both sides of the absorption envelope, a 2 nm shift in λ_{max}, and a decrease in intensity at λ_{max} (Figure 4A). Reaction of Y294H MauG with H_2O_2 results in a red-shift for only the higher energy side of the Soret band to produce a sharper feature, with a 1 nm shift in λ_{max} (Figure 4B) and similar decrease in intensity to that observed for reaction of WT MauG. Most significantly, addition of H_2O_2 to Y294H MauG results in the appearance of a broad absorption in the 600-700 nm range (Figure 4C) which is not observed with WT MauG. The difference spectrum of H_2O_2-treated minus diferric MauG shows a major peak centered at ~655 nm and a minor peak centered at ~600 nm. The appearance of these absorption peaks in the 600-700 nm region with an accompanying decrease in absorption in the Soret region are characteristic of Compound I (i.e., Fe(IV)=$O^{+\bullet}$) formation in heme-containing catalase, peroxidase and cytochrome P450 enzymes and model compounds (34-38). It should be noted that the decrease in intensity of the Soret peak of Y294H MauG after H_2O_2 addition is not as large as observed with some of the other heme proteins. In part this is because MauG is a diheme protein. Since the high valent species in the Y294H MauG is located on one heme, the Soret peak of only one of the two hemes will decrease. Thus, the magnitude of the observed absorbance change of the Soret region of the diheme protein is ~ 50% less than would be observed if it were possible to view only the Fe(IV)=$O^{+\bullet}$ heme. Furthermore, MauG is a *c*-type heme rather than a *b*-type heme which is typically involved in Compound I formation. It is conceivable that the covalent linkages to the protein could have an effect on the spectral features. It is noteworthy that spectral changes exhibited by Y294H MauG after H_2O_2 addition in both the Soret and high wavelength region are very similar to what was observed after H_2O_2 addition to the diheme cytochrome *c* peroxidase from *Nitrosomonas europaea* which were also attributed to Compound I formation (38).

This H_2O_2-induced spectral change for Y294H MauG occurred within the dead-time of mixing in the stopped-flow spectrophotometer as was also the case in formation of the *bis*-Fe(IV) state of WT MauG (26). The high valent Y294H MauG species was relatively stable and like the *bis*-Fe(IV) state of WT MauG decayed over several minutes with the rate of change in the spectral features in the 600-700 nm range approximating that of the rate of change in the Soret region (Figure 4D).

The nature of the high valent species formed after addition of H_2O_2 to Y294H MauG was further investigated using resonance Raman spectroscopy (Figure 5). The assignment of marker bands is based on the work of Spiro and coworkers (39). The resonance Raman

spectrum of diferric Y294H MauG exhibits two ν_2 bands at 1589 (low-spin) and 1570 cm^{-1} (high-spin), and a ν_3 band at 1506 cm^{-1} (low-spin) with a shoulder at ~1494 cm^{-1} (high-spin). After addition of H_2O_2, the high-spin marker bands at 1570 and 1494 cm^{-1} decrease, consistent with exogenous ligand binding to the five-coordinate heme iron. The ν_4 band at 1373 cm^{-1} is an empirical heme oxidation state marker. This band shifts 2 cm^{-1} to 1375 cm^{-1} after addition of H_2O_2. This shift is similar to what has been observed after addition of H_2O_2 to peroxidases and catalase (40-44). A difference spectrum (Figure 5) shows that the decrease in intensity of this peak is accompanied by increases of signal at 1358 cm^{-1} and 1381 cm^{-1}, which are characteristic signatures for Compound I and Compound II, respectively (40-42). While the presence of Compound II was not evident in the visible absorption spectrum, Compound I is known to be very sensitive to laser irradiation (40-42) and may have converted to Compound II during the laser excitation, which would be consistent with the appearance of the 1381 cm^{-1} band.

Effect of the Y294H Mutation on MauG-catalyzed TTQ Biosynthesis

It was previously shown that addition of preMADH to *bis*-Fe(IV) WT MauG causes a rapid return to the diferric species (see Scheme 1) with a rate of 0.8 s^{-1} as monitored by changes in the absorption spectrum in the region of the Soret peaks (26). In contrast, addition of preMADH to the high valent Y294H MauG species did not cause any increase over the slow rate of spontaneous return to the diferric state as judged by these spectral changes (Figure 6A). In steady state kinetic assays of TTQ biosynthesis (Scheme 1), MauG exhibits k_{cat} values of 0.2 s^{-1} with preMADH as the substrate (26) and 4.2 s^{-1} with quinol MADH as the substrate (28). When Y294H MauG was tested in these assays no detectable TTQ biosynthesis was observed with either preMADH (Figure 6B) or quinol MADH.

Effect of the Y294H Mutation on Electron Transfer from Diferrous MauG to Quinone MADH

In addition to the biosynthetic oxidation reactions described above which require formation of the *bis*-Fe(IV) MauG reaction intermediate (23,28), it was also demonstrated that thermodynamically favorable ET in the reverse direction of the biosynthetic reactions occurs from the diferrous MauG to quinone MADH (28). This reaction does not require formation of the *bis*-Fe(IV) state. Y294H MauG was active in this ET reaction despite being unable to catalyze TTQ biosynthesis (Figure 7). The K_d value for the reaction of quinone MADH with diferrous Y294H MauG (9.4 μM) is similar to that for WT MauG (10.1 μM, Table 2). The ET rate constant of 0.21 s^{-1} for the reaction with Y294H MauG is greater than that of 0.07 s^{-1} for the reaction with WT MauG.

Structure of the Y294H MauG/preMADH Complex

Diferric Y294H MauG was cocrystallized with preMADH and the X-ray crystal structure solved to a resolution of 1.92 Å, with a final R_{work} = 13.9 % and R_{free} = 18.7 % (Figure 8A). Data collection and refinement statistics are given in Table 3. The complex has the same overall structure as that reported previously for WT MauG/preMADH (PDB entry 3L4M), with the hemes and nascent TTQ site being coincident (15). The heme irons are 21 Å apart, with the mutation site heme iron being closest to the nascent TTQ at a distance of 19 Å from the closest precursor TTQ atom (Figure 8B). The asymmetric unit contains two crystallographically independent copies of Y294H MauG (Figure 8A), and within coordinate error the structural changes in the two copies are identical (RMSD of 0.36 Å for all atoms).

Although His has a smaller side-chain than Tyr, His294 is clearly ligated to the heme (Figure 9A). This results in a His-His coordination environment at the six-coordinate heme, with average bond distances of 2.1 Å for Fe–$N_{\varepsilon 2}$ His205 and 2.1 Å for Fe–N_{e2} His294. To support the ligand change, residues 291-314 in the C-terminal region of the Y294H MauG are displaced relative to WT MauG (RMSD in 291-314 Cα positions 1.37 Å and 0.75 Å, and

RMSD in all other Cα positions 0.20 Å and 0.16 Å for the two MauG copies (chains A and B respectively) in the asymmetric unit) (Figure 8B, 9B). This region starts within the helix (residues 286-298) containing the Y294H mutation site, with iron ligation by the shorter His294 side-chain tilting it in relation to the WT helix. At the C-terminal end of the helix the deviation in the backbone atoms between WT and Y294H reaches 2.6 Å. Maximal backbone differences of > 3.4 Å occur for residues 302 and 303 of chain A and residues 299 and 300 of chain B, which are part of a solvent exposed region of little secondary structure (298-314) (Figure 8B). The structural rearrangement of the protein observed in the mutant is peripheral, and does not impact the structure of the interface with preMADH or any protein structure between the redox centers within coordinate error. The preMADH nascent TTQ site, two MauG hemes, protein interface and residues in proximity to the proposed ET route are superimposable between the Y294H MauG/preMADH structure and that of WT MauG/preMADH. Thus, the only structural change caused by the mutation that seems relevant to TTQ biosynthesis is the replacement of the Tyr294 ligand with His.

Discussion

MauG is distinct from other heme proteins in its function and physical properties. It catalyzes successive, different oxidation reactions on amino acid residues of a substrate protein via long range electron/radical transfer (15,28). These oxidation reactions proceed via a *bis*-Fe(IV) intermediate in which the six-coordinate heme stabilizes the Fe(IV) state without an exogenous ligand (23). An unprecedented structural feature of MauG is that the six-coordinate *c*-type heme has His-Tyr axial ligation (15). The results presented here indicate that the Tyr294 axial heme ligand is critical for the unique reactivities of MauG.

Spectroscopic analysis of the reaction of Y294H MauG with H_2O_2 suggests that the six-coordinate heme of Y294H MauG, which has His-His axial ligation, cannot stabilize an Fe(IV) state. As a consequence, Y294H MauG does not form a stable *bis*-Fe(IV) state after addition of H_2O_2, but instead an alternative Fe(V)-equivalent state with spectral features characteristic of an Fe(IV)=O with an accompanying π radical which is present solely at the five-coordinate heme. Similar to the *bis*-Fe(IV) state of WT MauG, this Compound I-like state of Y294H MauG is relatively stable. However, it does not react with preMADH and Y294H MauG cannot catalyze TTQ biosynthesis from either preMADH or quinol MADH. The X-ray crystal structure of the Y294H MauG/preMADH complex shows that the inability to catalyze TTQ biosynthesis is not a consequence of general disruption of the protein structure, significant alterations of the Y294H MauG-preMADH interface, or any alteration of the heme structures and environment other than replacement of the Tyr axial ligand with His. ET from diferrous Y294H MauG to quinone MADH occurs with a comparable K_d and greater rate constant than in the reaction with WT MauG. This reverse ET reaction does not require the high valence state, only redox-active hemes, and these results confirm that ET between Y294H MauG and preMADH is possible. Additionally, generation of a high valent state alone, such as Compound I, is not sufficient for MauG-dependent TTQ biosynthesis. Thus, the biosynthetic oxidation reactions specifically require the *bis*-Fe(IV) state. Accordingly, the role of the *bis*-Fe(IV) state is not limited to providing a strong oxidant. The ability to stabilize the Fe(V)-equivalent over the two hemes, spanning a 21 Å separation, also significantly shortens the distance required for the long range electron transfer that is necessary for catalysis. The distance which separates the iron of the five-coordinate heme and the site of oxygen insertion into βTrp57 of preMADH is 44 Å (15). We have previously reported (28) that this distance from the nascent TTQ site of preMADH to the five-coordinate oxygen-binding heme is too great for direct ET to occur at the observed rates. However, it is possible in theory for this ET to occur via the six-coordinate heme. This is consistent with the need for the *bis*-Fe(IV) state that extends the

Fe(V) equivalent state to the six-coordinate heme rather than it being centered at the heme furthest from the nascent TTQ site.

Mutations of distal axial heme ligands are known to affect the redox properties of protein-bound hemes. Replacement of natural heme ligands with tyrosine has been shown to destabilize the Fe(II) state relative to the Fe(III) state (45), either as a consequence of decrease of the E_m value (46-48) or dissociation of the tyrosine from the iron upon reduction (49,50). The Y294H mutation of MauG affects both E_m values of the diheme redox system increasing the separation of the values such that it is much easier to add the first electron to Y294H MauG than to WT MauG, but then more difficult to add the second electron to Y294H MauG than to WT MauG. This result indicates that the ability in WT MauG to function coordinately as a diheme unit rather than independent hemes is not lost upon replacement of the Tyr heme ligand with His. This remarkable communication between the hemes also accounts for the observation that mutation of Tyr294, the distal ligand of the six-coordinate heme, resulted in a significant increase in the affinity of the five-coordinate heme for CO.

The demonstration of a critical role for Tyr294 in the function of MauG raises the question of why axial heme ligation by Tyr is so rare, and previously unknown in six-coordinate *c*-type hemes. The *c* hemes of cytochromes *c* typically function as ET mediators and do not participate in catalysis or oxygen activation (51). For a simple ET mediator there is no reason to stabilize an Fe(IV) redox state. In fact, to do so would be potentially harmful as the decay of the Fe(IV) state could lead to damage of the protein. As discussed earlier, naturally occurring mutations of an axial His ligand to Tyr has been shown to cause disease states in humans (12,13). Even for MauG, it was previously shown that generation of the *bis*-Fe(IV) state in the absence of substrate leads to inactivation (52). The unusual use of Tyr as a heme ligand for MauG seems to have evolved for the unusual catalytic function of this enzyme which requires stabilization of Fe(IV) on a six-coordinate heme.

Acknowledgments

We thank Elizabeth Graichen and Yu Tang for technical assistance and Dr. Aimin Liu and Jiafeng Geng for valuable discussion. We thank staff at sector 23, GM/CA-CAT, of the Advanced Photon Source, Argonne National Laboratory, Argonne, IL, USA for their assistance. GM/CA-CAT is funded by National Cancer Institute grant Y1-CO-1020 and National Institute of General Medical Sciences grant Y1-GM-1104. Use of the Advanced Photon Source was supported by the U.S. Department of Energy, Basic Energy Sciences, Office of Science, under contract DE-AC02-06CH11357. Computer resources were provided by the Basic Sciences Computing Laboratory of the University of Minnesota Supercomputing Institute, and we thank Can Ergenekan for support. We also thank Ed Hoeffner at the Kahlert Structural Biology Laboratory (KSBL) at the University of Minnesota.

References

1. Robinson DR, Wu YM, Lin SF. The protein tyrosine kinase family of the human genome. Oncogene. 2000; 19:5548–5557. [PubMed: 11114734]
2. Davidson VL. Protein-derived cofactors. Expanding the scope of post-translational modifications. Biochemistry. 2007; 46:5283–5292. [PubMed: 17439161]
3. Svistunenko DA, Cooper CE. A new method of identifying the site of tyrosyl radicals in proteins. Biophys. J. 2004; 87:582–595. [PubMed: 15240491]
4. Mayer JM, Rhile IJ, Larsen FB, Mader EA, Markle TF, DiPasquale AG. Models for proton-coupled electron transfer in photosystem II. Photosynth. Res. 2006; 87:3–20. [PubMed: 16437185]
5. MacMillan F, Kannt A, Behr J, Prisner T, Michel H. Direct evidence for a tyrosine radical in the reaction of cytochrome *c* oxidase with hydrogen peroxide. Biochemistry. 1999; 38:9179–9184. [PubMed: 10413492]
6. Stubbe J, van Der Donk WA. Protein radicals in enzyme catalysis. Chem. Rev. 1998; 98:2661–2662. [PubMed: 11848974]

7. Takahashi T, Yamashita H, Nakamura T, Nagano Y, Nakamura S. Tyrosine 125 of alpha-synuclein plays a critical role for dimerization following nitrative stress. Brain Res. 2002; 938:73–80. [PubMed: 12031537]
8. Giulivi C, Cadenas E. Heme protein radicals: formation, fate, and biological consequences. Free Radic. Biol. Med. 1998; 24:269–279. [PubMed: 9433902]
9. Cao C, Zhang Q, Wang ZQ, Wang YF, Wang YH, Wu H, Huang ZX. 1H NMR studies of the effect of mutation at Valine45 on heme microenvironment of cytochrome b_5. Biochimie. 2003; 85:1007–1016. [PubMed: 14644556]
10. Villegas JA, Mauk AG, Vazquez-Duhalt R. A cytochrome *c* variant resistant to heme degradation by hydrogen peroxide. Chem. Biol. 2000; 7:237–244. [PubMed: 10780923]
11. Bhaskar B, Immoos CE, Shimizu H, Sulc F, Farmer PJ, Poulos TL. A novel heme and peroxide-dependent tryptophan-tyrosine cross-link in a mutant of cytochrome *c* peroxidase. J. Mol. Biol. 2003; 328:157–166. [PubMed: 12684005]
12. Tsuda M, Kaneda M, Sakiyama T, Inana I, Owada M, Kiryu C, Shiraishi T, Kakinuma K. A novel mutation at a probable heme-binding ligand in neutrophil cytochrome b_{558} in atypical X-linked chronic granulomatous disease. Hum. Genet. 1998; 103:377–381. [PubMed: 9856476]
13. Cahilly C, Ballantyne CM, Lim DS, Gotto A, Marian AJ. A variant of p22(phox), involved in generation of reactive oxygen species in the vessel wall, is associated with progression of coronary atherosclerosis. Circ. Res. 2000; 86:391–395. [PubMed: 10700443]
14. Putnam CD, Arvai AS, Bourne Y, Tainer JA. Active and inhibited human catalase structures: ligand and NADPH binding and catalytic mechanism. J. Mol. Biol. 2000; 296:295–309. [PubMed: 10656833]
15. Jensen LM, Sanishvili R, Davidson VL, Wilmot CM. In crystallo posttranslational modification within a MauG/pre-methylamine dehydrogenase complex. Science. 2010; 327:1392–1394. [PubMed: 20223990]
16. Wang Y, Graichen ME, Liu A, Pearson AR, Wilmot CM, Davidson VL. MauG, a novel diheme protein required for tryptophan tryptophylquinone biogenesis. Biochemistry. 2003; 42:7318–7325. [PubMed: 12809487]
17. McIntire WS, Wemmer DE, Chistoserdov A, Lidstrom ME. A new cofactor in a prokaryotic enzyme: tryptophan tryptophylquinone as the redox prosthetic group in methylamine dehydrogenase. Science. 1991; 252:817–824. [PubMed: 2028257]
18. Davidson VL. Pyrroloquinoline quinone (PQQ) from methanol dehydrogenase and tryptophan tryptophylquinone (TTQ) from methylamine dehydrogenase. Adv. Protein Chem. 2001; 58:95–140. [PubMed: 11665494]
19. Pearson AR, De La Mora-Rey T, Graichen ME, Wang Y, Jones LH, Marimanikkupam S, Agger SA, Grimsrud PA, Davidson VL, Wilmot CM. Further insights into quinone cofactor biogenesis: probing the role of MauG in methylamine dehydrogenase tryptophan tryptophylquinone formation. Biochemistry. 2004; 43:5494–5502. [PubMed: 15122915]
20. Wang Y, Li X, Jones LH, Pearson AR, Wilmot CM, Davidson VL. MauG-dependent in vitro biosynthesis of tryptophan tryptophylquinone in methylamine dehydrogenase. J. Am. Chem. Soc. 2005; 127:8258–8259. [PubMed: 15941239]
21. Li X, Jones LH, Pearson AR, Wilmot CM, Davidson VL. Mechanistic possibilities in MauG-dependent tryptophan tryptophylquinone biosynthesis. Biochemistry. 2006; 45:13276–13283. [PubMed: 17073448]
22. Li X, Feng M, Wang Y, Tachikawa H, Davidson VL. Evidence for redox cooperativity between *c*-type hemes of MauG which is likely coupled to oxygen activation during tryptophan tryptophylquinone biosynthesis. Biochemistry. 2006; 45:821–828. [PubMed: 16411758]
23. Li X, Fu R, Lee S, Krebs C, Davidson VL, Liu A. A catalytic di-heme bis-Fe(IV) intermediate, alternative to an Fe(IV)=O porphyrin radical. Proc. Natl. Acad. Sci. U S A. 2008; 105:8597–8600. [PubMed: 18562294]
24. Davidson VL. Methylamine dehydrogenases from methylotrophic bacteria. Methods Enzymol. 1990; 188:241–246. [PubMed: 2126329]
25. Berry EA, Trumpower BL. Simultaneous determination of hemes *a*, *b*, and *c* from pyridine hemochrome spectra. Anal. Biochem. 1987; 161:1–15. [PubMed: 3578775]

26. Lee S, Shin S, Li X, Davidson VL. Kinetic mechanism for the initial steps in MauG-dependent tryptophan tryptophylquinone biosynthesis. Biochemistry. 2009; 48:2442–2447. [PubMed: 19196017]
27. Li X, Fu R, Liu A, Davidson VL. Kinetic and physical evidence that the diheme enzyme MauG tightly binds to a biosynthetic precursor of methylamine dehydrogenase with incompletely formed tryptophan tryptophylquinone. Biochemistry. 2008; 47:2908–2912. [PubMed: 18220357]
28. Shin S, Abu Tarboush N, Davidson VL. Long range electron transfer reactions between hemes of MauG and different forms of tryptophan tryptophylquinone of methylamine dehydrogenase. Biochemistry. 2010; 49:5810–5816. [PubMed: 20540536]
29. Otwinowski Z, Minor W. Processing of x-ray diffraction data collected by oscillation methods. Methods Enzymol. 1997; 276:307–326.
30. Murshudov GN, Vagin AA, Dodson EJ. Refinement of macromolecular structures by the maximum-likelihood method. Acta Crystallogr. Sect. D Biol. Crystallogr. 1997; 53:240–255. [PubMed: 15299926]
31. CCP4. Acta Crystallogr. Sect. D Biol. Crystallogr. 1994; 50:760–763. Collaborative Computational Project Number 4. [PubMed: 15299374]
32. Emsley P, Cowtan K. Coot: model-building tools for molecular graphics. Acta Crystallogr. Sect. D Biol. Crystallogr. 2004; 60:2126–2132. [PubMed: 15572765]
33. Fu R, Liu F, Davidson VL, Liu A. Heme iron nitrosyl complex of MauG reveals an efficient redox equilibrium between hemes with only one heme exclusively binding exogenous ligands. Biochemistry. 2009; 48:11603–11605. [PubMed: 19911786]
34. Makris TM, von Koenig K, Schlichting I, Sligar SG. The status of high-valent metal oxo complexes in the P450 cytochromes. J. Inorg. Biochem. 2006; 100:507–518. [PubMed: 16510191]
35. Sheng X, Horner JH, Newcomb M. Spectra and kinetic studies of the compound I derivative of cytochrome P450 119. J. Am. Chem. Soc. 2008; 130:13310–13320. [PubMed: 18788736]
36. Bell SR, Groves JT. A highly reactive P450 model Compound I. J. Am. Chem. Soc. 2009; 131:9640–9641. [PubMed: 19552441]
37. Dolphin D, Forman A, Borg DC, Fajer J, Felton RH. Compounds I of catalase and horse radish peroxidase: pi-cation radicals. Proc. Nat.l Acad. Sc.i U S A. 1971; 68:614–618.
38. Arciero DM, Hooper AB. A di-heme cytochrome c peroxidase from Nitrosomonas europaea catalytically active in both the oxidized and half-reduced states. J. Biol. Chem. 1994; 269:11878–11886. [PubMed: 8163487]
39. Hu S, Morris IK, Singh JP, Smith KM, Spiro TG. Complete assignment of cytochrome *c* resonance Raman spectra via enzymatic reconstitution, with isotopically labelled hemes. J. Am. Chem. Soc. 1993; 115:12446–12458.
40. Kincaid JR, Zheng Y, Al-Mustafa J, Czarnecki K. Resonance Raman spectra of native and mesoheme-reconstituted horseradish peroxidase and their catalytic intermediates. J. Biol. Chem. 1996; 271:28805–28811. [PubMed: 8910524]
41. Palaniappan V, Terner J. Resonance Raman spectroscopy of horseradish peroxidase derivatives and intermediates with excitation in the near ultraviolet. J. Biol. Chem. 1989; 264:16046–16053. [PubMed: 2777776]
42. Terner J, Palaniappan V, Gold A, Weiss R, Fitzgerald MM, Sullivan AM, Hosten CM. Resonance Raman spectroscopy of oxoiron(IV) porphyrin pi-cation radical and oxoiron(IV) hemes in peroxidase intermediates. J. Inorg. Biochem. 2006; 100:480–501. [PubMed: 16513173]
43. Chuang WJ, Heldt J, Van Wart HE. Resonance Raman spectra of bovine liver catalase compound II. Similarity of the heme environment to horseradish peroxidase compound II. J. Biol. Chem. 1989; 264:14209–14215. [PubMed: 2547789]
44. Kitagawa T, Mizutani Y. Resonance Raman spectra of highly oxidized metalloporphyrins and heme proteins. Coord. Chem. Rev. 1994; 135/136:685–735.
45. Goodwin DC, Rowlinson SW, Marnett LJ. Substitution of tyrosine for the proximal histidine ligand to the heme of prostaglandin endoperoxide synthase 2: implications for the mechanism of cyclooxygenase activation and catalysis. Biochemistry. 2000; 39:5422–5432. [PubMed: 10820014]

46. Nagai M, Yoneyama Y. Reduction of methemoglobins M Hyde Park, M Saskatoon, and M Milwaukee by ferredoxin and ferredoxin-nicotinamide adenine dinucleotide phosphate reductase system. J. Biol. Chem. 1983; 258:14379–14384. [PubMed: 6643489]

47. Adachi S, Nagano S, Watanabe Y, Ishimori K, Morishima I. Alteration of human myoglobin proximal histidine to cysteine or tyrosine by site-directed mutagenesis: characterization and their catalytic activities. Biochem. Biophys. Res. Commun. 1991; 180:138–144. [PubMed: 1930211]

48. Hildebrand DP, Burk DL, Maurus R, Ferrer JC, Brayer GD, Mauk AG. The proximal ligand variant His93Tyr of horse heart myoglobin. Biochemistry. 1995; 34:1997–2005. [PubMed: 7849057]

49. Farver O, Kroneck PM, Zumft WG, Pecht I. Allosteric control of internal electron transfer in cytochrome cd_1 nitrite reductase. Proc. Natl. Acad. Sci. U S A. 2003; 100:7622–7625. [PubMed: 12802018]

50. Liu Y, Moenne-Loccoz P, Hildebrand DP, Wilks A, Loehr TM, Mauk AG, Ortiz de Montellano PR. Replacement of the proximal histidine iron ligand by a cysteine or tyrosine converts heme oxygenase to an oxidase. Biochemistry. 1999; 38:3733–3743. [PubMed: 10090762]

51. Bertini I, Cavallaro G, Rosato A. Cytochrome *c*: occurrence and functions. Chem. Rev. 2006; 106:90–115. [PubMed: 16402772]

52. Shin S, Lee S, Davidson VL. Suicide inactivation of MauG during reaction with O_2 or H_2O_2 in the absence of its natural protein substrate. Biochemistry. 2009; 48:10106–10112. [PubMed: 19788236]

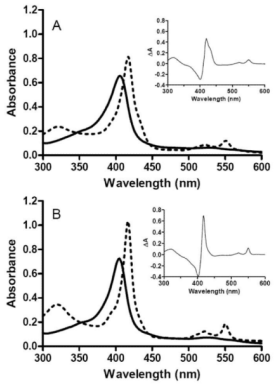

Figure 1.

Absorption spectra of oxidized and reduced WT MauG (A) and Y294H MauG (B). The spectra of the diferric (solid lines) and diferrous (dashed lines) forms were recorded in 50 mM potassium phosphate, pH 7.5. Reduced-oxidized difference spectra are shown in the insets.

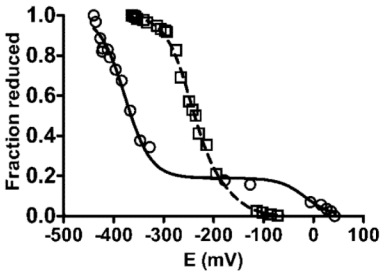

Figure 2.

Spectrochemical redox titrations of WT MauG (squares) and Y294H MauG (circles). Titrations were performed anaerobically in 50 mM potassium phosphate, pH 7.5, as described under Experimental Procedures. Solid lines are fits of the data to eq 1.

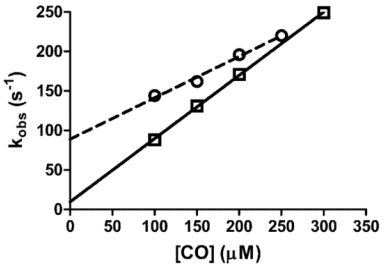

Figure 3.

Reactions of diferrous WT MauG (dashed line) and Y294H MauG (solid line) with CO. Rates were determined by stopped-flow spectroscopy as described under Experimental Procedures. The rates of the faster, [CO]-dependent major phase of the reaction are plotted and data were fit to a linear regression analysis.

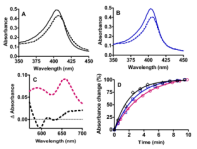

Figure 4.

Changes in the absorption spectra of WT and Y294H MauG upon addition of H_2O_2. (A) Soret region of WT MauG (1.7 μM) before (solid line) and after (dashed line) addition of H_2O_2. (B) Soret region of Y294H MauG (1.5 μM) before (solid line) and after (dashed line) addition of a stoichiometric amount of H_2O_2. (C) Difference spectra (immediately after H_2O_2 addition minus diferric spectra) of the higher wavelength region of the spectra for WT MauG (black) and Y294H MauG (red). In each case 15 μM protein was mixed with 15 μM H_2O_2. (D) Time course of spontaneous return of the absorption spectrum after H_2O_2 addition to that of the diferric protein; WT MauG at 406 nm (black diamonds), Y294H MauG at 404 nm (blue squares) and Y294 MauG at 655 nm (red circles).

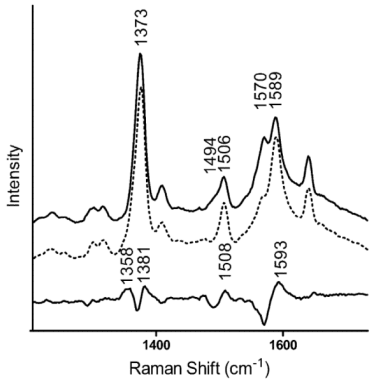

Figure 5.

Changes in the resonance Raman spectrum of Y294H MauG upon addition of H_2O_2. Overlaid are the resonance Raman spectra of diferric Y294H MauG before (solid line) and after (dashed line) reaction with a stoichiometric amount of H_2O_2. The bottom trace is the H_2O_2-treated minus diferric difference spectrum. Spectra were recorded in the frozen state with 0.2 mM protein in 10 mM potassium phosphate, pH 7.5.

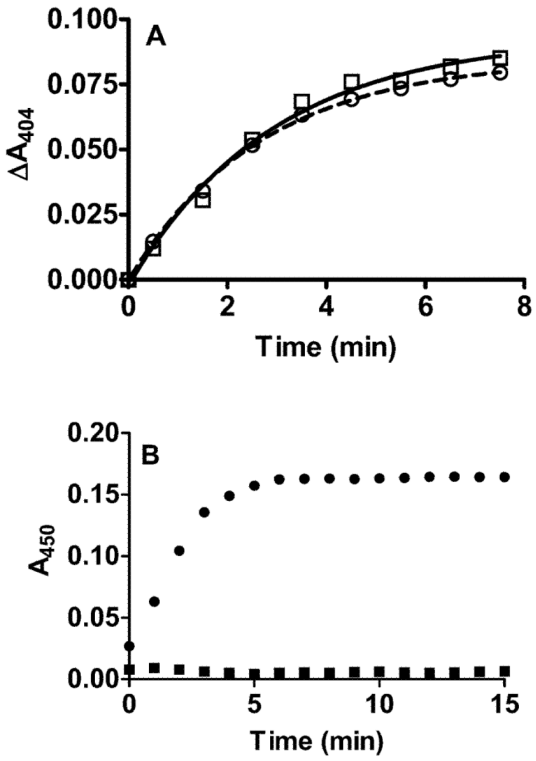

Figure 6.

Lack of reaction of Y294H MauG with preMADH. (A) Time course of the return of the absorption spectrum after H_2O_2 addition to Y294H MauG that of the diferric protein in the absence (squares) and presence (circles) of preMADH. (B) Steady state reaction of WT MauG (circles) and Y294H MauG (squares) with preMADH as a substrate. Experiments were performed as described in the text and the formation of TTQ was monitored 450 nm.

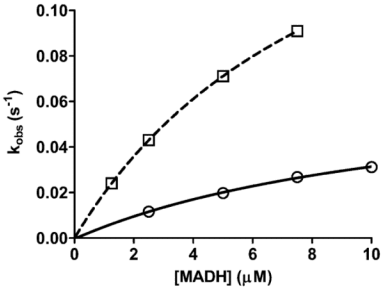

Figure 7.

Single-turnover kinetics of the reactions of diferrous WT MauG (solid line) and Y294H MauG (dashed line) with quinone MADH. The lines represent fits of the data to eq 3.

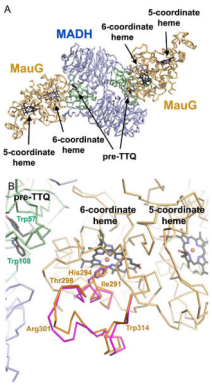

Figure 8.

Overall structure of the Y294H MauG/preMADH complex and comparison of the C-terminal regions of Y294H MauG and WT MauG. (A) Cα trace of the Y294H MauG/preMADH structure. (B) Overlay of Cα traces for the C-terminal regions of Y294H MauG and WT MauG that exhibit significant differences. The protein Cα trace, heme and pre-TTQ are drawn as stick and colored by atom (carbon: Y294H MauG yellow; α-preMADH pale blue; β-preMADH green; hemes and nascent TTQ dark grey). The iron is shown as an orange sphere. Residues 289–316 of WT MauG are shown as a Cα trace in magenta. The figure was produced using PyMOL (http://www.pymol.org/).

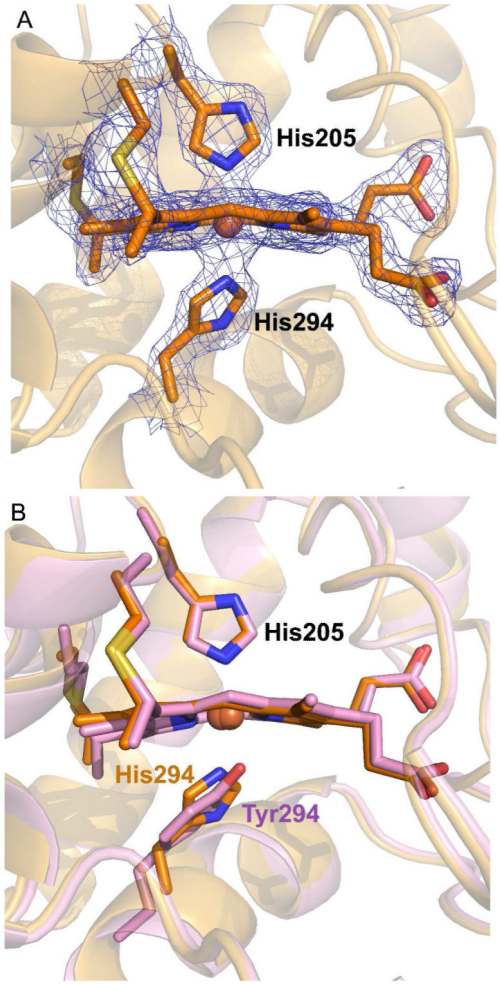

Figure 9.

The six-coordinate hemes of Y294H MauG and WT MauG. (A) 2Fo-Fc electron density (blue mesh contoured at 2.0 σ) at the six-coordinate heme of Y294H MauG. (B) Overlay of Y294H MauG and WT MauG coordinates. The protein is drawn as cartoon (Y294H MauG yellow; WT MauG pink). The hemes, Cys201 and Cys204 (thioether linkages) and axial ligands are drawn in stick colored by atom (carbon: Y294H MauG orange; WT MauG pink). The figure was produced using PyMOL (http://www.pymol.org/).

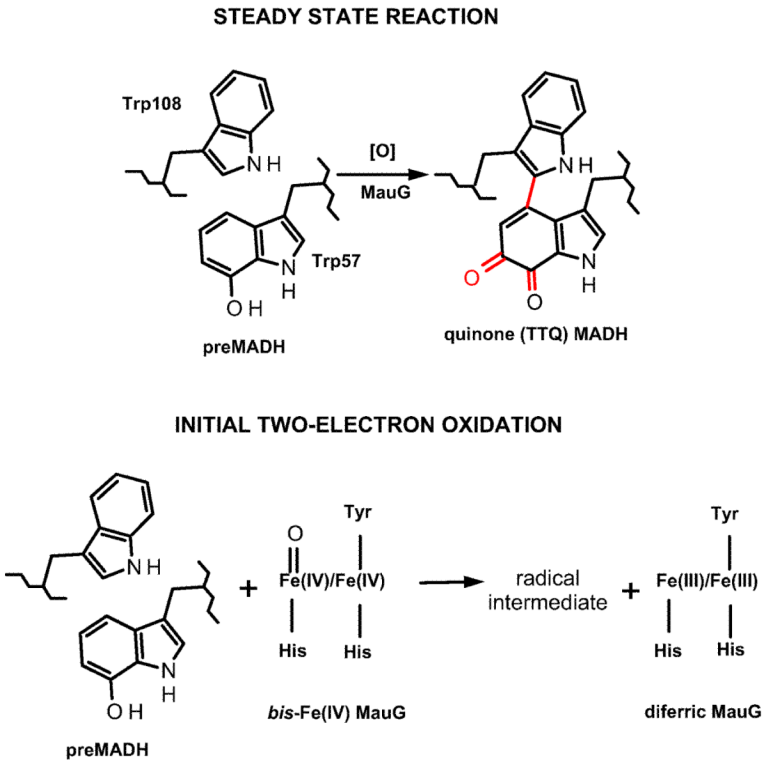

Scheme 1.

Table 1

Effects of the Y294H mutation on absorption maxima (λ_{max}) and extinction coefficients (ε) of MauG

Redox state	λ_{max} (ε) nm ($mM^{-1}cm^{-1}$)	
	MauG	Y294H MauG
Diferric	406 (309)	404 (347)
Diferrous	418 (327)	416 (434)
	524 (34)	522 (39)
	552 (50)	550 (66)
High valent	407 (271)	406 (286)
	-	655 (8.5)

Table 2

Effects of the Y294H mutation on redox properties and reactivity of MauG

Properties	WT MauG	Y294H MauG
E_m values (mV)	− 158 ± 9 −246 ± 3	−17 ± 13 −377 ± 2
CO binding: k_{on} ($M^{-1}s^{-1}$) k_{off} (s^{-1}) K_d (μM)	(5.2±0.4) × 10^5 88 ± 8 168 ± 19	(8.0 ±0.1) × 10^5 9.4 ± 2.5 12 ± 3.2
k_{cat} for TTQ biosynthesis from preMADH (s^{-1})	0.2[a]	0
k_{cat} for TTQ biosynthesis from quinol MADH (s^{-1})	4.2[b]	0
Electron transfer rate from diferrous MauG to quinone MADH (s^{-1})	0.07 ± 0.01[b]	0.21 ± 0.01
K_d for diferrous MauG-quinone MADH complex (μM)	10.1 ± 1.6[b]	9.4 ± 0.1

[a] Value for WT MauG were taken from reference (27)

[b] Values for WT MauG were taken from reference (26)

Table 3

X-ray crystallography data collection and refinement statistics.[b]

Data collection	**Y294H-MauG/preMADH**
Detector type	MAR*mosaic* 4×4 tiled CCD
Source	APS, Sector 23
Space group	*P*1
Unit cell lengths (Å)	55.53 × 83.52 × 107.78
Unit cell angles (°)	109.94, 91.54, 105.78
Wavelength (Å)	1.03325
Resolution (Å)	50.00 – 1.92 (1.95 – 1.92)
Measured reflections	469, 801
Unique reflections	126, 251
Completeness (%)	95.6 (70.6)
R_{merge} (%)[b]	8.0 (42.5)
I/σI	13.6 (2.0)
Multiplicity	3.7 (2.2)
Refinement	
Resolution (Å)	44.49 – 1.91 (1.96 – 1.91)
No. reflections; working/test	119, 911/6, 318
R_{work} (%)[c]	13.9
R_{free} (%)[d]	18.7
Protein atoms	13, 288
Ligand atoms	262
Solvent sites	1301
Ramachandran statistics[e]	
Allowed (%)	99.23
Outliers (%)	0.77
Root mean square deviation	
Bond lengths (Å)	0.025
Bond angles (°)	2.078
Average B-factor (Å^2)	28.72
ESU (Å)[f]; R_{work}/R_{free}	0.137/0.131
PDB code	30 RV

[a] Values in parentheses are for the highest resolution shell.

[b] $R_{merge} = \Sigma_i |I_{hkl,i} - \langle I_{hkl} \rangle| / \Sigma_{hkl} \Sigma_i I_{hkl,i}$, where I is the observed intensity and $\langle I_{hkl} \rangle$ is the average intensity of multiple measurements.

[c] $R_{work} = \Sigma||F_O|-|F_C|| / \Sigma|F_O|$, where $|F_O|$ is the observed structure factor amplitude, and $|F_C|$ is the calculated structure factor amplitude.

[d] R_{free} is the R factor based on 5% of the data excluded from refinement.

[e] Based on values attained from refinement validation options in COOT (32)

[f] Estimated standard uncertainties generated for R_{work} and R_{free} in Refmac5.5 (30) in the CCP4 suite (31).